

Content from this work may be used under the terms of the CC BY 3.0 licence (© 2018). Any distribution of this work must maintain attribution to the author(s), title of the work, publisher, and DOI.

DESIGN AND FEA OF AN INNOVATIVE ROTATING SiC FILTER FOR HIGH-ENERGY X-RAY BEAM

W. Tizzano*, T. Connolley, S. Davies, M. Drakopoulos, G. E. Howell
 Diamond Light Source, OX11 0DE Didcot, United Kingdom

Abstract

I12 Joint Engineering, Environmental, and Processing (JEEP) is a high-energy imaging, diffraction and scattering beamline at Diamond. Its source is a superconducting wiggler with a power of approximately 9 kW at 500 mA after the fixed front-end aperture; two permanent filters aim at reducing the power in photons below the operating range of the beamline of 50-150 keV, which accounts for about two-thirds of the total [1]. This paper focuses on the design and simulation process of the secondary permanent filter, a 4 mm thick SiC disk. The first version of the filter was vulnerable to cracking due to thermally induced stress, so a new filter based on an innovative concept was proposed: a water-cooled shaft rotates, via a ceramic interface, the SiC disk; the disk operates up to 900 °C, and a copper absorber surrounding the filter dissipates the heat through radiation. We utilised analysis data following failure of an initial prototype to successfully model the heat flow using FEA. This model informed different iterations of the re-design of the assembly, addressing the issues identified. The operational temperature of the final product matches within a few degrees Celsius the one predicted by the simulation.

example engineering parts and assemblies (e.g., superalloy turbine blades [2], or steel and Al alloy internal combustion engines [3]). Table 1 summarizes the key parameters of the beamline and Fig. 1 shows its layout.

Table 1: I12 Key Parameters [4]

Source	Super-conducting wiggler, 4.2 T, 48 mm periodicity, 22 full field periods
Beam acceptance	1 mrad×0.3 mrad
Beam modes	White beam or monochromatic beam
Monochromator	Si (111) cryo-cooled double crystal bent Laue
Energy range	50–150 keV

INTRODUCTION

I12 is a high-energy imaging, diffraction and scattering beamline located on a straight section of Diamond storage ring. Its source is a 4.2 T superconducting wiggler, and the beamline operates at 50–150 keV, providing a hard X-ray beam capable of penetrating large dense samples, for

The techniques available to I12 users include, among the others: static and time-resolved radiography and tomography, energy-dispersive diffraction, monochromatic and white-beam two-dimensional diffraction/scattering, and high energy Small-Angle X-ray Scattering (SAXS) [1].

The beamline has two in-line experimental hutches (EH), one inside Diamond Experimental Hall 51.7 m from the source (EH1), and the other in an external building 94.5 m from the source (EH2). EH1 allows experiments involving small and medium-sized samples and sample environments, whereas EH2 offers space for large or complex experiments [5].

* walter.tizzano@diamond.ac.uk

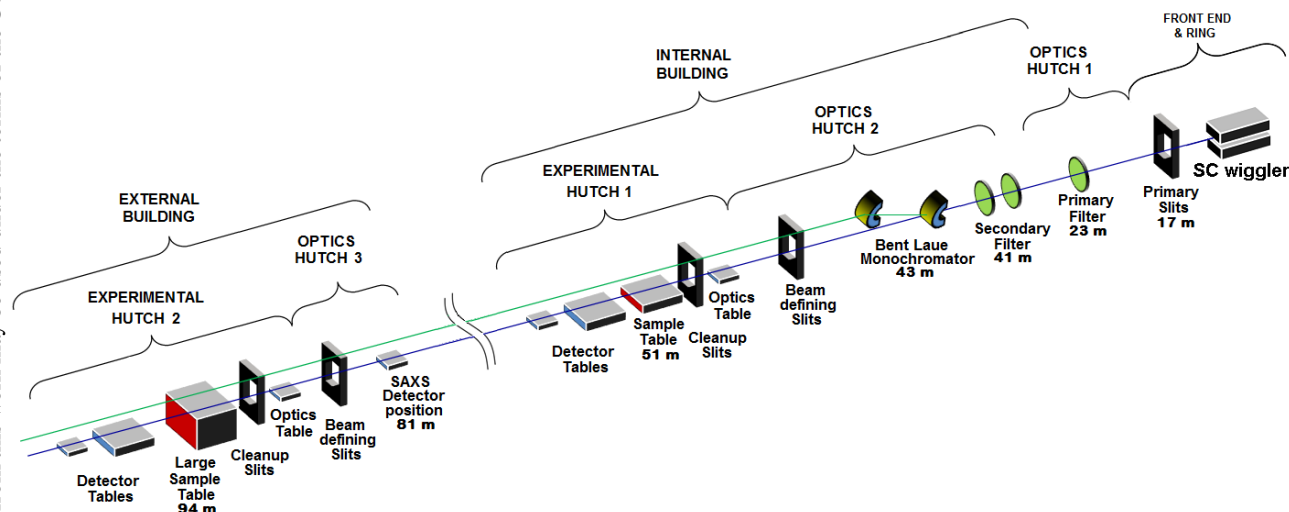


Figure 1: Schematic optical and functional layout of the I12 JEEP beamline [4].

HEAT LOAD MANAGEMENT

Diamond Light Source Storage Ring currently operates at 300 mA [6], with design intent up to 500 mA [7]. With this current, the total power emitted by the wiggler would be 56 kW, and the maximum power entering the beam line through the fixed front-end aperture would be 9 kW [1].

About two-thirds of this power is due to photons below the operating range of the beamline of 50-150 keV, and for this reason two permanent filters are installed upstream of the Laue monochromator (see Fig. 1). The primary filter is a series of two water-cooled Chemical Vapour Deposited (CVD) diamond disks, that reduce the total power to 6.2 kW. This paper will focus mainly on the secondary filter, that aims at reducing the power from 6.2 kW to 2.6 kW. Figure 2 shows the flux at 500 mA, and the effect of the aforementioned filters and of attenuators of different thickness.

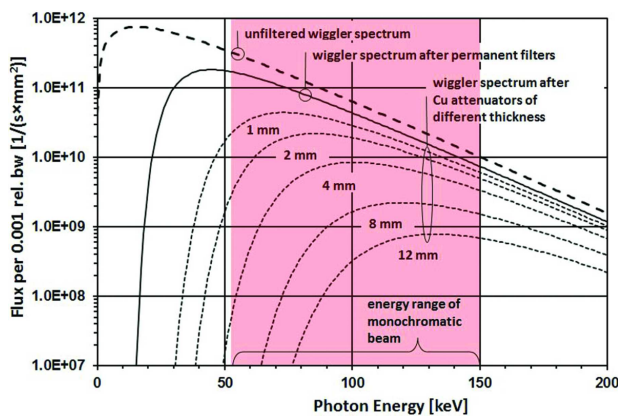


Figure 2: Photon flux at 500 mA calculated with XOP [8], in the full 1 mrad×0.3 mrad fan accepted by the beamline at 50 m from the source. The effect of filters and attenuation is shown [1].

Static Secondary Filter

The beamline was initially commissioned with a static secondary filter, consisting in a 4 mm thick SiC disk, diffusion bonded to a water cooled Cu carrier via a Mo interface (see Fig. 3).

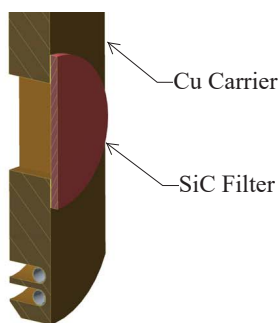


Figure 3: Static filter.

A combination of thermally-induced stress and residual stress from the diffusion bonding [1] proved to be too challenging for the filter. Following failure on first aperture of maximum beam load at 300 mA, it was necessary to replace

it with a completely different design, that would not have diffusion bonding and that would be less vulnerable to thermal stresses.

Rotating Secondary Filter

A new assembly filter, shown in Fig. 4, was designed. In this design, the SiC disk rotates at 60 RPM, in this way the thermal load is distributed on a larger area, reducing the power density the filter material is subjected to. Two Cu water-cooled absorbers collect the heat radiated by the filter; the rotating shaft (that is also water-cooled) dissipates the remaining thermal power, transmitted conductively through a series of Machinable Glass Ceramic (MACOR®) and titanium alloy parts.

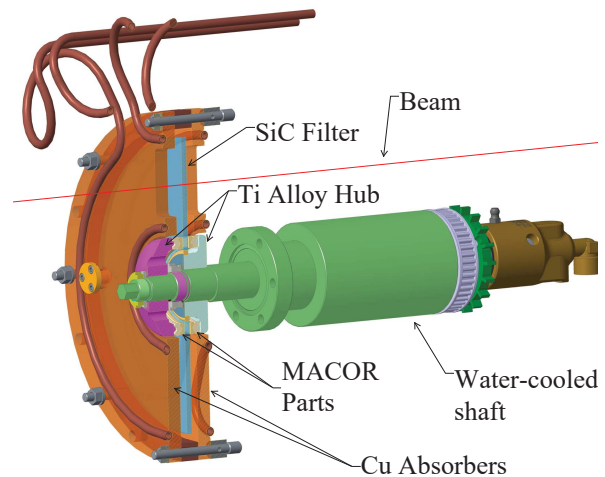


Figure 4: First prototype of the rotating filter.

A thermal finite element simulation was performed, and it showed that no part was subjected to excessive temperatures or stresses, so a first prototype was made and tested; however, the temperatures measured were higher than the ones predicted, and the ceramic parts exhibited some cracking. Further analysis was required.

FAILURE ANALYSIS

The fact that the temperature was higher than predicted suggests that the system exhibited more internal thermal resistance than the one assumed in the simulation, as the boundary conditions are known with a good degree of precision. In particular, the boundary conditions for this system are represented by the external thermal load, accurately calculated by XOP, and the convective water cooling, whose characteristic parameter h was estimated analytically with well-established formulas¹. As for the internal thermal resistance, it can be represented with the electrical circuit analogy², as shown in Fig. 5.

T_d represents the maximum SiC Disk temperature, T_w the cooling water temperature, R_{cond} is a resistance equivalent

¹ The equation for convection is $\dot{Q} = hA\Delta T$, where \dot{Q} is the thermal power, h is the convective heat transfer coefficient, A is the heat transfer area and ΔT is the temperature difference between the bulk fluid and the

Content from this work may be used under the terms of the CC BY 3.0 licence (© 2018). Any distribution of this work must maintain attribution to the author(s), title of the work, publisher, and DOI.

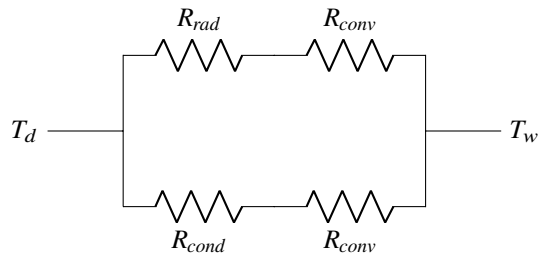


Figure 5: Circuit analogy.

to the parallel of two series of conductive resistances the heat must go through to reach the water cooled shaft, R_{conv} models the convection heat transfer, and R_{rad} is a resistance that takes into account the effect of radiation, governed (for grey bodies³) by this law:

$$\dot{Q} = \frac{\sigma(T_d^4 - T_a^4)}{\frac{1 - \epsilon_d}{A_d \epsilon_d} + \frac{1}{A_d F_{d \rightarrow a}} + \frac{1 - \epsilon_a}{A_a \epsilon_a}}, \quad (1)$$

where d and a are respectively the SiC disk and absorber surfaces interested to the radiation phenomenon, T is their temperature, ϵ their emissivity, A their area, and $F_{d \rightarrow a}$ the view factor from the disk to the absorber.

The fact that T_d from the simulation was significantly lower than the one measured during the test, suggests that either R_{rad} or R_{cond} was higher than the one in the simulation. R_{rad} was estimated with a sufficient degree of precision⁴, so by exclusion it could be assumed that the most significant source of error was likely to be R_{cond} .

As mentioned above, R_{cond} is in fact equivalent to a parallel of two series of resistances. These resistances depend on the conductivity of the materials, their geometry and the interface between them. The materials used are well known, and their conductivity can easily be found on reputable material databases, like MatWeb [11], and the geometry error is negligible, as it depends only on small manufacturing tolerances and some small approximations due to the mesh. This means that the error was probably due mostly by how the interface between the parts was modeled.

At the interface between two parts in contact along a thermal conductance path, there is a temperature drop due to the Thermal Contact Resistance (TCR). This depends on several factors, like the contact pressure between the two parts, the materials, the surface roughness etc. Figure 6

shows how the TCR changes with contact pressure for some common interstitial materials. By default, ANSYS assigns to this variable a very small value⁵, that can be considered like a 'perfect' contact, which is one where there is practically no temperature drop.

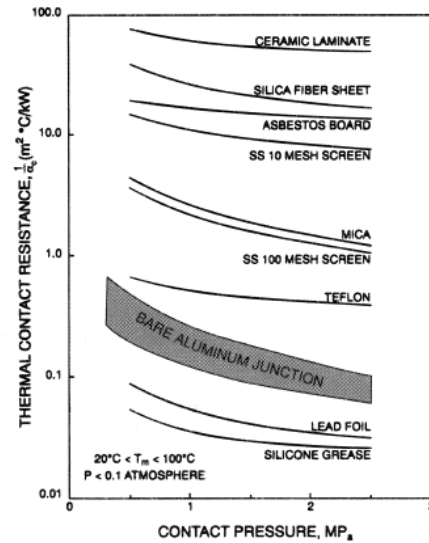


Figure 6: Contact resistance for selected interstitial materials for thermal enhancement or thermal isolation [12].

Even if tables and graphs are available in the literature (e.g., [14]), it is not easy to identify the value of the TCR for all the interfaces in the assembly, because some of the variables it depends on are not known. An alternative approach is to isolate the interface effects from the conductance through the single parts and add a resistor in our electrical model, as shown in Fig. 7. Such a resistor is variable, and by changing its value we change the calculated T_d , if all the other variables are unchanged.

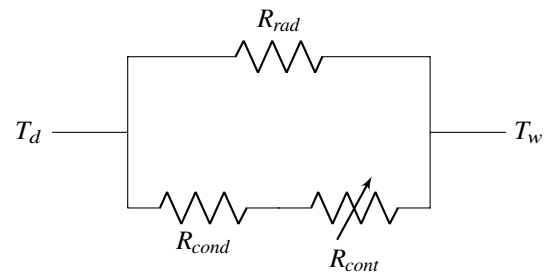


Figure 7: Circuit analogy that takes into account the TCR (R_{conv} omitted for clarity).

By varying R_{cont} until T_d matched the one measured during the test, we could identify a value of this parameter that takes into account the collective effect of all the contact interfaces in the model. In this way we could estimate how much

surface. For forced convection, the parameter h can be estimated with empirical formulas available in the literature [9].
² Ohm's law ($V_2 - V_1 = RI$) can be used in thermal circuits as $(T_2 - T_1) = R\dot{Q}$, where T_1 and T_2 are the temperatures of two points of the system, R is the thermal resistance between them, and \dot{Q} is the thermal power transferred from one point to the other.
³ An approximation according which ϵ is frequency independent.
⁴ It depends on the geometry of the parts and the emissivity ϵ of the materials interested to the radiative heat exchange. For the copper absorbers, a conservative value of $7 \cdot 10^{-2}$ [10] was used, whereas the SiC disk's emissivity was measured using the cold immersion method by a Land M1 thermometer having a spectral response of $1.6 \mu\text{m}$. The measured value was 0.66 ± 0.2 at 700°C and did not vary significantly with temperature.

⁵ $TCC = K_{xx} 10^3 / ASM_{diag}$, where TCC is the thermal contact conductance, the reciprocal of TCR, K_{xx} is the largest material conductivity defined in the model, and ASM_{diag} is the geometry bounding box diagonal [13].

heat is transferred by radiation and how much by conduction. In electrical terms, estimate the relative contribution of the two branches of our circuit.

The prototype was tested with a heat load of 389 W, and a model that uses the default value for the TCR predicted a T_d of $\approx 590^\circ\text{C}$ (see Fig. 8a), which means that almost 60% of the thermal power would be dissipated conductively (the lower branch of Fig. 7). The temperature measured in the test was however significantly higher ($\approx 780^\circ\text{C}$, see Fig. 8b), and the R_{cont} that makes the calculated FEA equal to this value is $5\text{ m}^2\text{C/kW}$. Taking into account the TCR , according to the simulation, only 11% of the power is transferred conductively, which explains the higher temperature reached by the disk⁶.

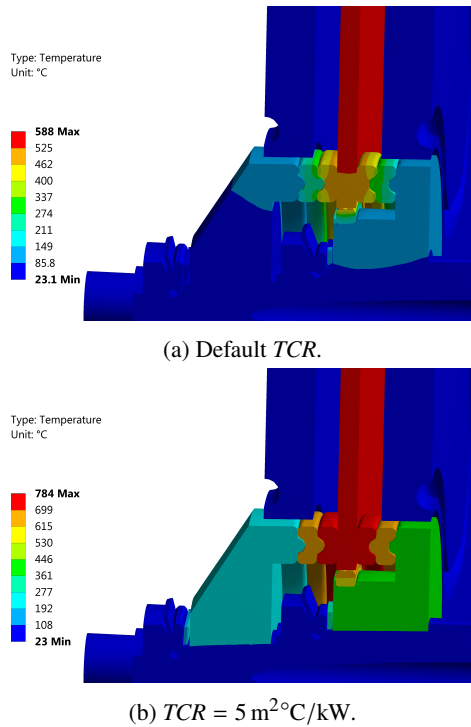


Figure 8: Simulations on the prototype with default (8a) and custom (8b) values for the TCR .

The thermal contact resistance calculated above is relatively high, but realistic, for ceramic parts. It is unacceptably high for metal parts, unless the contact pressure is extremely poor. This suggests that the interface between the Ti alloy hubs and the steel shaft did not transfer sufficient heat because there was not enough contact pressure between these components. One way to improve this is to use the Axiomatic Design principles.

Axiomatic Design

Axiomatic Design is a powerful design methodology that divides the Design World into four domains, and

⁶ The total heat load staying the same, all the heat that is not transferred by conduction must be radiated by the disk to the Cu absorbers; hence, if more heat is transferred in this way, the temperature of the disk must be higher, in accordance to Eq. (1).

models the relationships between them with matrices. The four domains are the Customer domain, the Functional domain, the Physical domain, and the Process domain. To each of these a characteristic vector is assigned ($\{CA_s\}, \{FR_s\}, \{DP_s\}, \{PV_s\}$). The method takes its name from the fact that it is based on two axioms⁷ [15]:

1. the Independence Axiom;
2. the Information Axiom.

The Independence Axiom says that the Functional Requirements should be independent. This means that if we express the relationship between Functional Requirements $\{FR_s\}$ and the Design Parameters $\{DP_s\}$ as $\{FR_s\} = [A]\{DP_s\}$, the matrix $[A]$ should be diagonal. If the design matrix $[A]$ is not diagonal, the $\{FR_s\}$ are coupled, and optimising a Design Parameter to achieve a Functional Requirement might affect other Functional Requirements too, making the optimisation harder, sometimes impossible and the design less robust⁸.

The Information Axiom says that the information content of the design should be minimised⁹.

If we consider the subassembly that includes the water-cooled shaft and the titanium alloy hubs, we have two Functional Requirements:

- $\{FR_1\}$ - can assemble;
- $\{FR_2\}$ - transfers heat.

We have however only a single Design Parameter, the difference between the hub internal diameter D_h and the shaft external diameter d_s that we can call x . We can represent this in matrix form as follows:

$$\begin{Bmatrix} FR_1 \\ FR_2 \end{Bmatrix} = \begin{bmatrix} a_{1,1} & 0 \\ a_{2,1} & 0 \end{bmatrix} \begin{Bmatrix} x \\ 0 \end{Bmatrix} \quad (2)$$

The matrix $[A]$ is not diagonal, hence the design is not uncoupled¹⁰; x affects both $\{FR_1\}$ and $\{FR_2\}$, but its optimal value is different for the two Functional Requirements: to make assembly easier, we want a low contact pressure, but to transfer heat we need a high contact pressure. There is a contradiction¹¹.

One way to resolve this contradiction is to follow the first axiom, and modify our system so that the matrix $[A]$ is diagonal and our system is hence uncoupled.

⁷ Self-evident statements that cannot be derived from other principles.
⁸ There is also a third possibility: the matrix $[A]$ can be triangular. In this case, the system is decoupled, which is a non-ideal scenario but still preferable to a coupled system.
⁹ The *information content* I is defined as $I = \log_2 1/P$, and it represents the probability of satisfying a given functional requirement [15].
¹⁰ All systems with more $\{FR_s\}$ than $\{DP_s\}$ are coupled.
¹¹ Also, x is temperature dependent: the greater the ΔT between hubs and shaft, the greater the TCR become, which leads to even higher ΔT . This causes a runaway phenomenon where temperature spirals out of control.

FINAL DESIGN

The analysis of the failed prototype informed the final design, that addressed the weaknesses we identified, and that were described in the previous sections. In particular, changes were made to improve the heat transfer between the hubs and the shaft without compromising the ease of assembly, and to maximise the heat dissipated through radiation.

Redesigned Hubs

A feature was added to the hubs, consisting in some wedges that allow the tightening of the hub around the shaft after it has been slid into position, as shown in Fig. 9.

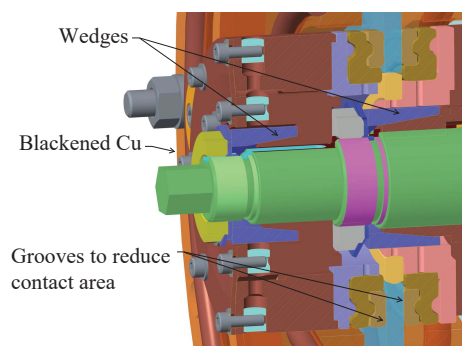


Figure 9: Final Design.

This allows for both easy installation and high contact pressure during operation. In axiomatic design terms, the new feature gives us another design parameter that we can call y , hence the system now looks like this:

$$\begin{Bmatrix} FR_1 \\ FR_2 \end{Bmatrix} = \begin{bmatrix} a_{1,1} & 0 \\ 0 & a_{2,2} \end{bmatrix} \begin{Bmatrix} x \\ y \end{Bmatrix} \quad (3)$$

In the redesigned assembly x has a different meaning, and it represents the clearance of the wedges before they are compressed. y is the clamping force and depends on the wedge geometry (height, angle etc.)¹². The matrix $[A]$ is now diagonal, and the system uncoupled¹³.

Maximising Radiation

If a 389 W heat load radiation heat transfer dominated (only 11% was transferred conductively), this would be even more true with higher heat loads (the heat transferred by radiation grows with the fourth power of temperature (Eq. (1)), the one transferred by conduction only grows linearly with the temperature¹⁴). For this reason, we decided to increase the radiation heat transfer by improving the emissivity ϵ of the copper absorbers. This could be achieved by blackening

¹² Similarly to x in the first prototype, also y varies with ΔT . However, in this case, the clamping force grows with ΔT ; consequently the TCR becomes smaller, which leads to a stable thermal equilibrium.

¹³ By design there is clearance between the uncompressed wedges and the shaft. If we had interference, the term $A_{2,1}$ would be different from 0, and our system would be decoupled.

¹⁴ $\dot{Q} = U\Delta T$, where U is the conductance.

them¹⁵. Also, we wanted to increase the conductive resistance of the chain of components supporting the disk, so that less heat would be transferred along that path. We achieved this by considerably reducing the contact surface between the ceramic parts and the disk (by adding some grooves on the ceramic, in the positions indicated in Fig. 9).

FEA

The redesigned assembly was simulated, using the thermal contact resistance value estimated with the prototype¹⁶. With a calculated thermal load of 3.6 kW at 500 mA, the predicted disk temperature is $\approx 880^\circ\text{C}$ (see Fig. 10). Diamond is currently operating at 350 mA, so the maximum condition cannot be validated with a physical measurement.

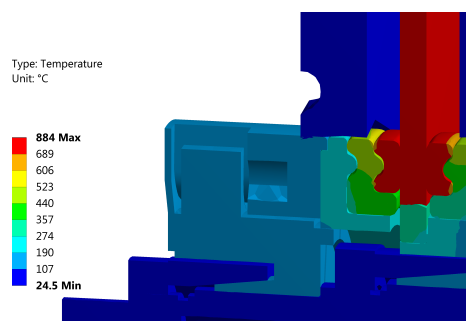


Figure 10: Thermal FEA on the final design, with the maximum 500 mA current in the storage ring.

For this reason, we simulated the assembly with other heat loads, and compared the results with the values measured in the operational assembly. The simulation is able to predict reliably and conservatively the temperatures: the error is less than 10%, and the simulated value is always larger than the measured one, confirming that the assumptions made were conservative. Also, the heat is now dissipated almost exclusively by the absorbers, as only $\approx 1\%$ goes to the water-cooled shaft¹⁷.

CONCLUSION

The redesigned rotating SiC filter has been installed in August 2016, and it has been used from September 2016 onward, with the fixed filter still in place downstream. The rotating filter has been operating since then without showing any problem. For this reason, in December 2017 the fixed filter has been removed, and we have been using just the rotating one since January 2018. We can conclude that the final design, informed by the thermal FEA described in the sections above, is robust and effective.

REFERENCES

[1] M. Drakopoulos *et al.*, "I12: the Joint Engineering, Environment and Processing (JEEP) beamline at Diamond Light

¹⁵ By heating the copper in air, the surface is covered by CuO (cupric oxide), a black solid compound with high ϵ , stable at room temperature.

¹⁶ The geometry was modified to improve that value, so using it is a conservative assumption.

¹⁷ For medium-high heatloads. For low heat-loads this value is higher.

Content from this work may be used under the terms of the CC BY 3.0 licence (© 2018). Any distribution of this work must maintain attribution to the author(s), title of the work, publisher, and DOI.

- Source”, in *Journal of Synchrotron Radiation* (2015), vol. 22, pp. 828–838, doi:10.1107/S1600577515003513
- [2] N. Baimpas, M. Xie, C. Reinhard, and A. Korsunsky, “The application of geometry corrections for Diffraction Strain Tomography (DST) analysis of a Ni-base superalloy blade”, in *Powder Diffraction*, Sep. 2013, vol. 28, pp. S436–S447, doi:10.1017/S0885715613000857
- [3] N. Baimpas *et al.*, “A feasibility study of dynamic stress analysis inside a running internal combustion engine using synchrotron X-ray beams”, in *Journal of Synchrotron Radiation* (2013), vol. 20, pp. 316–323, doi:10.1107/S0909049513000885
- [4] Diamond Light Source, I12 Beamline Characteristics <http://www.diamond.ac.uk/Beamlines/Engineering-and-Environment/I12/Beamline-Characteristics.html>
- [5] Diamond Light Source, Introduction to I12 – JEEP <http://www.diamond.ac.uk/Beamlines/Engineering-and-Environment/I12.html>
- [6] Diamond Light Source, Storage Ring Status <http://www.diamond.ac.uk/default/MachineStatus.html>
- [7] C. Christou *et al.*, “Implications of Increased Beam Current for the Diamond Storage Ring Rf System”, presented at the 16th International Conference on RF Superconductivity, SRF 2013.
- [8] M. Sanchez del Rio and R. J. Dejus, “Status of XOP: an x-ray optics software toolkit”, in *Proc. SPIE 5536, Advances in Computational Methods for X-Ray and Neutron Optics*, vol. 5536, 21 October 2004, doi:10.1117/12.560903
- [9] W. M. Kays, *Convective Heat and Mass Transfer*, McGraw-Hill Education; 4th edition (May 1, 2004).
- [10] Mikron, Table of Emissivity of Various Surfaces http://www-eng.lbl.gov/~dw/projects/DW4229_LHC_detector_analysis/calculations/emissivity2.pdf
- [11] MatWeb <http://www.matweb.com>
- [12] L. K. Fletcher, “Review of Thermal Control Materials for Metallic Junctions”, in *Journal of Spacecraft and Rockets*, vol. 9, n. 12 (1972), pp. 849–850, doi:10.2514/3.61809
- [13] *Thermal Analysis*, ANSYS, in ANSYS Training Manual.
- [14] L. J. Salerno and P. Kittel, “Thermal Contact Conductance”, in *NASA Technical Memorandum 110429*.
- [15] N. P. Suh, “Axiomatic Design: Advances and Applications”, *New York: Oxford University Press*, 2001. ISBN: 0195134664.